Development of the Leeuwin Current on the northwest shelf of Australia through the Pliocene-Pleistocene period

Yuxin He [a,*], Huanye Wang [b], Zhonghui Liu [c]

[a] *Key Laboratory of Geoscience Big Data and Deep Resource of Zhejiang Province, School of Earth Sciences, Zhejiang University, Hangzhou 310027, China*
[b] *State Key Lab of Loess and Quaternary Geology, Institute of Earth Environment, CAS, Xi'an 710061, Shaanxi, China*
[c] *Department of Earth Sciences, The University of Hong Kong, Hong Kong, China*

A B S T R A C T

Although the Leeuwin Current (LC) is thought to play a pivotal role in climatic and oceanic systems of the western Australian region, how the LC developed through the Pliocene-Pleistocene period remains elusive. Here we used biomarker records to reconstruct variations of temperatures and primary productivity on the northwest shelf of Australia over the last 6 million years. Since ∼1.2 million years ago (Ma), our sea surface temperature record indicates progressive warming, with temperature values comparable to those in the Indo-Pacific Warm Pool, in contrast with the long-term global cooling trend. The regional surface warming was accompanied by suppressed primary productivity, together indicating prevailing warm, low-salinity, nutrient-deficient surface water, and thus a stronger LC since the Mid-Pleistocene Transition. During 4–1.2 Ma, greater surface temperature gradient between the Indo-Pacific Warm Pool and the northwest shelf of Australia and higher primary productivity seem to suggest a generally weaker LC. Warmer temperatures and lower productivity suggest a plausible existence of the LC during 6–4 Ma, but more work is required to confirm this. Impact of sea level and the Indonesian Throughflow on the LC strength may exist, but did not dominate through the Pliocene-Pleistocene period, considering different variation patterns among them. We propose the stronger LC after ∼1.2 Ma was more likely triggered by enhanced atmospheric circulation. Although the increased LC after ∼1.2 Ma may have potentially brought additional moisture to the Australian continent during the interglacial periods, it has not overturned the long-term drying trend through the Pliocene-Pleistocene period.

© 2021 Elsevier B.V. All rights reserved.

1. Introduction

Oceanic conditions and climates of the northwestern Australian region are largely influenced by variations in the Indonesian Throughflow (ITF) and the Leeuwin Current (LC), especially over the Pliocene-Pleistocene period (Cane and Molnar, 2001; Molnar and Cronin, 2015; Sniderman et al., 2016). As an important component of the global thermohaline conveyor, the ITF transports water and heat from the western Pacific Ocean into the eastern Indian Ocean, and is a major source for the LC on the northwest shelf of Australia (Gordon, 2005). The shallow and narrow LC (<100 km wide, <300 m deep), which is the only southward-flowing eastern boundary current in the Southern Hemisphere, transports warm and fresh tropical water against the equatorward wind stress, coastal upwelling and the northward-flowing West Australia Current, resulting in additional warm sea surface tem-perature (SST) on the northwest shelf of Australia (Morrow et al., 2003; Pattiaratchi, 2006; Feng et al., 2015). The LC modifies pole-ward heat transport in the Indian Ocean and moisture availability on the semi-arid northwestern Australian continent (Molnar and Cronin, 2015). Therefore, the evolution of LC strength is impor-tant to our understanding of climatic and oceanic systems of the western Australian region.

Earth has experienced a major transition from the warm Pliocene with slightly warmer SST in the Western Pacific Warm Pool but substantially weaker meridional and zonal SST gradients of the Pacific Ocean, to the cooler Pleistocene (Fedorov et al., 2013; Zhang et al., 2014; Herbert et al., 2016). Through the Pliocene, ongoing ITF constriction has been attributed to emergence of the Maritime Continent caused by sea level changes and tectonic re-organization of the Indonesian Gateway system (Cane and Molnar, 2001; Krebs et al., 2011). Recently, several studies from the In-ternational Ocean Discovery Program (IODP) Expedition 356 have made important contributions on pinning down the timing of the ITF constriction and its climatic effect on the Australian continent. Based on records from Sites U1459 and U1463, reductions of the

ITF strength at ~3.7 million years ago (Ma) in response to a tectonic reorganization of the Maritime Continent, and at ~3.3 Ma in response to a sea level drop, were identified (Christensen et al., 2017; De Vleeschouwer et al., 2018, 2019; Auer et al., 2019, 2020; Smith et al., 2020). These tectonic reorganizations are thought to have caused a long-term cooling and drying out of the northwestern Australia (Sniderman et al., 2016; Christensen et al., 2017; Stuut et al., 2019).

During the Pleistocene when the ITF was tectonically restricted, records of the ITF and LC strengths are relatively sparse. An early study focusing on microfossil biogeographic connectivity between the western Pacific Ocean and the northwest shelf of Australia suggested relatively stronger ITF and LC during 1.6–0.8 Ma (Gallagher et al., 2009). Recently, based on TEX_{86} temperature records derived from glycerol dialkyl glycerol tetraethers (GDGTs) at Site U1460, Petrick et al. (2019) proposed cooling and weak ITF conditions at ~0.65 and ~1.55 Ma, which were caused by global sea level lowering and regional tectonic changes. Records of TEX_{86} and long-chain diol temperatures from Site U1463 also show a strong cooling condition at ~1.7–1.5 Ma caused by a significant step in the ongoing ITF constriction (Smith et al., 2020). However, the TEX_{86} proxy may contain some degree of subsurface signal (Smith et al., 2013; Ho and Laepple, 2016; Kim et al., 2016), and the relation of the LC and the ITF might be complicated when the ITF is relatively weak. Accordingly, variation of the LC and its potential triggers through the Pliocene-Pleistocene period remain elusive and require further investigation.

As the LC transports warm, low-salinity, nutrient-deficient tropical surface water along the west coast of Australia (Pattiaratchi, 2006), abnormally warm sea surface and suppressed primary productivity can be used as indicators of stronger LC conditions. Alkenone-based $U^{K'}_{37}$-SST proxy has been widely used in a variety of marine environments (e.g. Prahl et al., 1988; Müller et al., 1998). Concentrations of isoprenoid GDGTs (isoGDGTs) and C_{28}–C_{30} sterols can be indicators of primary productivity of archaea (Schouten et al., 2013) and algae (Volkman et al., 1998), respectively. Here we reconstruct 6-million-year-long records of alkenone- and GDGT-based temperatures, and primary productivity from IODP Site U1461 on the northwest shelf of Australia (Fig. 1). By combining information of sea temperatures and primary productivity, development of the LC and its impacts on the climates of the northwestern Australian region through the Pliocene-Pleistocene period can be inferred.

2. Materials and methods

2.1. Cores at Site U1461

Site U1461 (20°12′51″S, 115°03′56″E, water depth of 126 m, Figs. 1, S1) is located ~100 km northwest of Barrow Island. Four major units were identified in the sedimentary cores at Site U1461 (Fig. S2; Gallagher et al., 2017). Unit I (Hole U1461B = 0–11.3 m core depth below seafloor) consists of unlithified gray wackestone with benthic foraminifers and bivalves. Unit II (Hole U1461B = 11.3–466.4 m) consists of coarse-grained, dark-colored, unlithified wackestone/packstone and fine-grained, light-colored unlithified mudstone. The lower section of Unit II (U1461B = ~330–466 m) was formed very quickly due to the Gorgon Slide tectonic event, and was excluded from the chronological profile (Fig. S2). Unit III (U1461B = 466.4–877.6 m) consists of lithified greenish gray to olive-gray wackestone. Unit IV (Hole U1461D = 992.9–1088.9 m) consists of lithified, light greenish gray, fine sand-sized packstone that grades into creamy gray coarse sand-sized packstone.

The chronological profile for the cores at Site U1461 was built by datums from biostratigraphy, micropaleontology, lithological property and ^{14}C dates (Table S2, Fig. S2). Based on ^{14}C dates
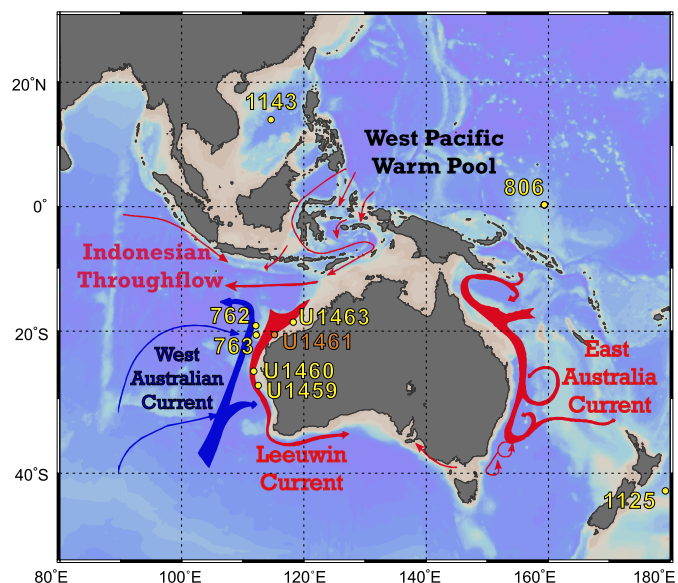
Fig. 1. Modern oceanography (created by the software of Ocean Data View) and ocean circulation in the Indo-Pacific and Australian regions (adapted from Gallagher et al., 2009). Orange dot indicates the position of Site U1461 and yellow dots indicate the positions of Sites 762, 763, 806, 1125, 1143, U1459, U1460, and U1463. Warm surface currents were shown in red arrows while cold surface currents in blue arrows. (For interpretation of the colors in the figure(s), the reader is referred to the web version of this article.)

of macrofossils and planktonic foraminifera, sediments at 0–11 m mainly cover the Holocene and the Last Glacial Maximum (Ishiwa et al., 2019). For sediments at 11–245 m, we further assigned some datums to the Marine Isotopic Stages (MIS) based on the lithological property, considering light-colored sediments were developed under cool and arid conditions in which high alkalinity favors carbonate precipitation (Gallagher et al., 2018; Hallenberger et al., 2019). For instance, relatively dark sediments at 40–50 m and 63–100 m are assigned to be from the MIS 5e and the MIS 7, while light-colored sediments at 50–63 m from the MIS 6 (Gallagher et al., 2017). For sediments at 245–950 m, we assigned datums from planktonic foraminifers and calcareous nannofossils (Gallagher et al., 2017; Table S2). The chronological profile for sediments at 0–950 m was built by linear interpolation between these datums (Fig. S2). Based on the current chronology, our $U^{K'}_{37}$ and TEX_{86} values are roughly correlated with the globally distributed benthic $\delta^{18}O$ records on orbital scales over the last 3 million years (Myr, Fig. S3; Lisiecki and Raymo, 2005). The chronological profile for sediments at 950–1086 m was built by linear extrapolation of the datums at 900 m and 950 m (Fig. S2), which is reasonable as these sediments belong to the early Pliocene and the late Miocene according to the calcareous nannofossil record (Gallagher et al., 2017).

2.2. Biomarker analysis

We chose sediments from Holes A, B, and D for biomarker analysis, and no obvious offset was found in the biomarker records among these holes (Fig. S4). Total lipids were obtained from ~20 g freeze-dried sediments by ultrasonic extraction with dichloromethane:methanol (9:1, v/v) for at least 3 times. The total lipids were then hydrolyzed with 6% KOH in methanol solution to remove alkenoates that could interfere the identification of alkenones. The neutral fraction containing alkenones, sterols and archaeal ether lipids was extracted by *n*-hexane from the hydrolyzed lipids. The neutral fraction was analyzed on an Agilent 7890B Gas Chromatograph with an Agilent 5977 Mass Spectrometer for identification of alkenones and sterols (Fig. S5), and on an

Agilent 7890B Gas Chromatography with a Flame Ionization Detector for quantitation of alkenones and C_{28}–C_{30} sterols using the internal (n-Tetracosane-d_{50}) and external standards (cholesterol). The Gas Chromatograph was equipped with a DB-1MS capillary column (60 m × 0.32 mm × 0.25 μm) with 1 mL/min Helium carrier flow. The oven temperature program is: hold at 80 °C for 2 min, increase to 310 °C at 15 °C/min, and hold at 310 °C for 40 min. In some samples during 1.25–1.15 Ma (21 samples) and 6–4.5 Ma (18 samples), no identifiable alkenones or trace alkenone occurrence with bad chromatograph were observed. We reported these samples as no alkenones detected to ensure the data quality (Table S1).

The neutral fraction was re-dissolved in hexane/isopropanol (99:1, v/v), filtered with 0.45 μm glass-fiber filter, and further analyzed for archaeal ether lipids by a Shimadzu LC-MS 8030 high-performance liquid chromatography–mass spectrometry. Separation of archaeal ether lipids was obtained with an Inertsil SIL-100A silica column (250 mm × 4.6 mm, 3 μm) at 40 °C using isopropanol and n-hexane as elutes for pump A and pump B, respectively. The total flow rate of pump A and pump B was maintained at 0.4 mL/min. The solvent program for gradient of pump B is: decrease linearly from 97% to 86% at 0–38 min, decrease linearly from 86% to 0% at 38–39 min, hold at 0% at 39–46 min, increase linearly from 0% to 97% at 46–47 min, and hold at 97% at 47–60 min. Archaeal ether lipids were ionized in the atmospheric pressure chemical ionization source at an interface temperature of 350 °C, a desolvation line temperature of 280 °C, and a heating block temperature of 250 °C, with the nebulizing gas and drying gas at 2.5 L/min and 5 L/min, respectively. Quantification was performed by integration of the peak area of ions in the extracted ion chromatograms, and comparison to the C_{46} external standard.

The alkenone-based $U_{37}^{K'}$ and C_{37}/C_{38} values were calculated with the following equations:

$$U_{37}^{K'} = [C_{37:2}]/([C_{37:2}] + [C_{37:3}]) \quad \text{(Prahl et al., 1988)}; \tag{1}$$

$$C_{37}/C_{38} = ([C_{37:2}] + [C_{37:3}])/([C_{38:2}] + [C_{38:3}])$$

$$\text{(Prahl et al., 1988)}; \tag{2}$$

where $[C_{n:2}]$ and $[C_{n:3}]$ are concentrations of di- and tri-unsaturated C_n alkenones (n = 37, 38).

There is no regional calibration between $U_{37}^{K'}$ and SST for the northwest shelf of Australia. We then derived the mean annual SST according to the equation based on cultural calibration from strain 55a of *Emiliania huxleyi* (equation (3); Prahl et al., 1988), which is very close to the global calibration (Müller et al., 1998).

$$SST = 29.41 \times U_{37}^{K'} - 1.15 \quad \text{(Prahl et al., 1988)}. \tag{3}$$

The GDGT-based TEX_{86}, BIT (branched versus isoprenoid tetraether index), and MI (methane index) values were calculated with the following equations:

$$TEX_{86} = ([GDGT\text{-}2] + [GDGT\text{-}3] + [Cren'])$$
$$/([GDGT\text{-}1] + [GDGT\text{-}2] + [GDGT\text{-}3] + [Cren']) \tag{4}$$
$$\text{(Schouten et al., 2002)};$$

$$BIT = ([GDGT\text{-}Ia] + [GDGT\text{-}IIa] + [GDGT\text{-}IIIa])$$
$$/([GDGT\text{-}Ia] + [GDGT\text{-}IIa] + [GDGT\text{-}IIIa] + [Cren]) \tag{5}$$
$$\text{(Hopmans et al., 2004)};$$

$$MI = ([GDGT\text{-}1] + [GDGT\text{-}2] + [GDGT\text{-}3])$$
$$/([GDGT\text{-}1] + [GDGT\text{-}2] + [GDGT\text{-}3] + [Cren] + [Cren']) \tag{6}$$
$$\text{(Zhang et al., 2011)};$$
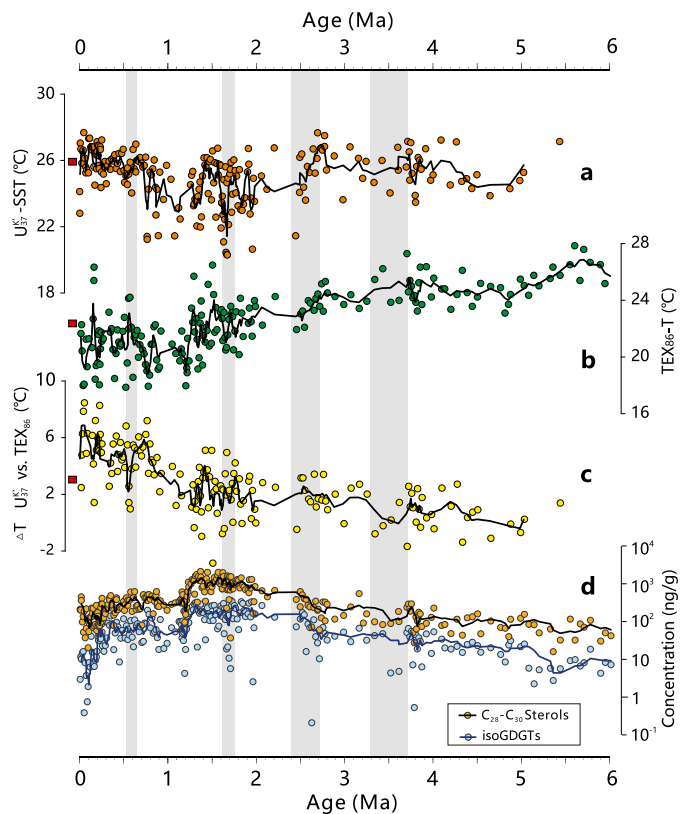
Fig. 2. Temperatures and primary productivity at Site U1461 on the northwest shelf of Australia over the last 6 Myr. (a) $U_{37}^{K'}$-based SST with 3-point smoothing curve. (b) TEX_{86}-based temperature with 3-point smoothing curve. (c) Vertical thermal difference between $U_{37}^{K'}$-based SST and TEX_{86}-based temperature with 3-point smoothing curve. (d) Concentrations of isoGDGTs (blue dots) and C_{28}-C_{30} sterols (orange dots) with 3-point smoothing curves. Red squares indicate the modern annual value of SST (a), temperature at 100 m depth (b), and their difference (c) at Site U1461 derived from HadSST3 Dataset (https://www.metoffice.gov.uk/hadobs/hadsst3/). Gray shadings indicate some cooling events proposed by previous studies (Auer et al., 2019; De Vleeschouwer et al., 2019; Petrick et al., 2019; Smith et al., 2020).

where [Cren], [Cren′], and [GDGT-X] are concentrations of crenarchaeol, crenarchaeol isomer, and GDGT-X (X = 1, 2, 3, Ia, IIa, and IIIa).

In this study, we interpreted the TEX_{86} as an indicator of temperature of the whole water column (see discussion below). At present, there are no regional temperature calibration for the northwest shelf of Australia. We derived a temperature calibration (equation (7)) for TEX_{86} with a simple linear regression from global datasets collected by Tierney and Tingley (2014).

$$\text{Temperature}(TEX_{86}) = 58.44 \times TEX_{86} - 17.04 \tag{7}$$

Analytical uncertainty for quantification of these biomarkers would be less than 5%, and all the ratio-based proxies are only minorly impacted by this analytical uncertainty. The large range of concentrations of these biomarkers, much greater than the analytical uncertainty, indicates that there is no issue with interpretation of these biomarkers within Site U1461 (Fig. 2, Table S1). The potential uncertainties derived from the temperature calibrations of $U_{37}^{K'}$ and TEX_{86} are independent of discussing the temperature gradients between sites and their assessment of LC variation. Potential error might occur when calculating the difference between the $U_{37}^{K'}$-based and TEX_{86}-based temperatures at Site U1461. However, after comparing a number of calibrations for converting $U_{37}^{K'}$ and TEX_{86} values to temperatures (Prahl et al., 1988; Müller et al., 1998; Schouten et al., 2013; Tierney and Tingley, 2014; Kim et al.,

2016), we suggest that our choice of calibrations for both $U_{37}^{K'}$ and TEX$_{86}$ would only have limited impacts on the absolute temperature values.

2.3. Temperature gradient calculation

To avoid uncertainties in different temperature proxies (Lawrence and Woodard, 2017), calculation for the temperature gradient between sites was conducted only on an internally consistent proxy dataset. For the temperature gradient, we calculated the difference of the temperature proxies ($U_{37}^{K'}$ and TEX$_{86}$) by their absolute values, and then transformed them into temperature difference according to the temperature calibrations (equations (3) and (7)). In this way, uncertainties in different calibrations applied in the cited studies can be avoided. On the northwest shelf of Australia, we calculated the TEX$_{86}$ temperature difference between Site U1461 and Site U1460 during 2.6–0 Ma (Petrick et al., 2019), and Site U1461 and Site U1459 during 5–2 Ma (De Vleeschouwer et al., 2019; Fig. 3c). $U_{37}^{K'}$-SST difference between Site ODP 806 (Zhang et al., 2014) and Site U1461 was calculated to represent the SST gradient between the Indo-Pacific Warm Pool and the northwest shelf of Australia (Fig. 3a). SST difference between Site ODP 1143 in the South China Sea (Li et al., 2011) and Site U1461 was also calculated as a supplementary record for the SST gradient between the Indo-Pacific Warm Pool and the northwest shelf of Australia (Fig. 3a), considering very low resolution of the $U_{37}^{K'}$ record at Site 806 (Zhang et al., 2014). SST difference between Site U1461 and Site ODP 1125 to the east of New Zealand (Caballero-Gill et al., 2019; Peterson et al., 2020) was calculated to represent SST gradient between the northwest shelf of Australia and the higher latitude region (Fig. 3b). Although Site 1125 is not in the west shelf of Australia (Fig. 1), it is currently our best choice for the $U_{37}^{K'}$ record from high latitude Southern Hemisphere. More work on the SST records in higher latitude area from west shelf of Australia is important to further address this issue in the future.

3. Results

3.1. $U_{37}^{K'}$-SSTs on the northwest shelf of Australia

Over the last 6 Myr, $U_{37}^{K'}$-SSTs at Site U1461 vary from 20.3 to 27.7 °C (Fig. 2a, Table S1). $U_{37}^{K'}$-SST values at the near-shore Site U1461 are similar with Mg/Ca-SST values from the off-shore Site ODP 763 during 5–3.5 Ma, but ∼2 °C warmer than Site 763 during 3–2.5 Ma (Karas et al., 2011; Fig. S6). Two possible reasons can explain why these two SST records diverge. Firstly, it is possible that Site 763 more closely tracks Indian Ocean signal rather than an ITF signal after ∼3 Ma (De Vleeschouwer et al., 2018). Secondly, the different SSTs might be caused by the nature of uncertainties between the two SST proxies (Mg/Ca vs. $U_{37}^{K'}$), which is quite common in Pliocene-Pleistocene SST records around the world (Lawrence and Woodard, 2017).

During 6–1.2 Ma, the $U_{37}^{K'}$-SSTs at Site U1461 decreased gradually at a rate of 0.5 °C/Myr, similar with the general global cooling trend over the Pliocene-Pleistocene period (Lisiecki and Raymo, 2005; Zhang et al., 2014; Herbert et al., 2016; Fig. S6). At some well-recognized cooling and ITF weakening periods including 1.55, 2.55, and 3.7–3.3 Ma (De Vleeschouwer et al., 2018, 2019; Auer et al., 2019, 2020; Petrick et al., 2019), $U_{37}^{K'}$-SSTs at Site U1461 also decreased (Fig. 2a). After ∼1.2 Ma, $U_{37}^{K'}$-SSTs at Site U1461 increased by ∼4 °C (Fig. 2a), in contrast with the global cooling trend (Lisiecki and Raymo, 2005; Zhang et al., 2014; Herbert et al., 2016; Fig. S6).
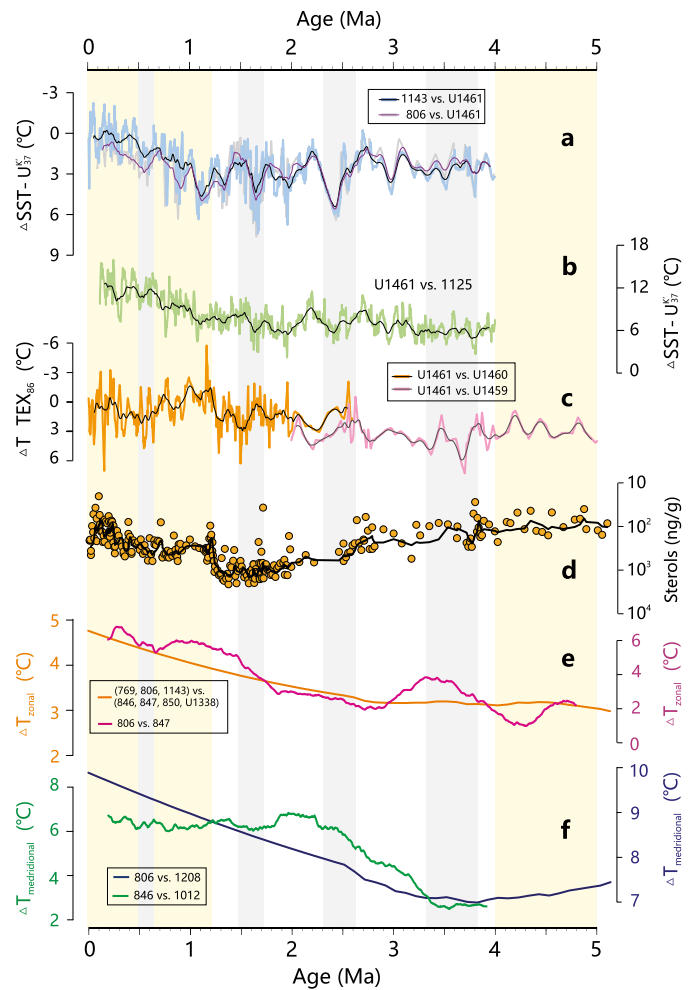
Fig. 3. Temperature settings on the northwest shelf of Australia over the last 5 Myr. (a) Differences of $U_{37}^{K'}$-based SST between Site 1143 (Li et al., 2011) and Site U1461 (blue lines with black 0.1 Ma smoothing curves), and between Site 806 (Zhang et al., 2014) and Site U1461 (gray lines with purple 0.1 Ma smoothing curves) over the last 4 Myr. (b) Difference of $U_{37}^{K'}$-based SST between Site U1461 and Site 1125 (Caballero-Gill et al., 2019; Peterson et al., 2020) over the last 4 Myr (green lines with black 0.1 Ma smoothing curves). (c) Differences of TEX$_{86}$-based temperature between Site U1461 and Site U1460 during 2.6–0 Ma (orange lines with black 0.1 Ma smoothing curves, Petrick et al., 2019), and between Site U1461 and Site U1459 during 5–2 Ma (pink lines with gray 0.1 Ma smoothing curves, De Vleeschouwer et al., 2019). (d) Concentrations of C_{28}–C_{30} sterols from Site U1461 with 3-point smoothing curve over the last 5 Myr (in reversed scale). (e) Zonal temperature gradients of the Pacific Ocean based on different methods (Site 806 vs. Site 847, Fedorov et al., 2013; Sites 769, 806, 1143 vs. Sites 846, 847, 850, U1338, Zhang et al., 2014). (f) Meridional temperature gradients of the Pacific Ocean based on different methods (Site 806 vs. Site 1208, Fedorov et al., 2013; Site 846 vs. Site 1012, Zhang et al., 2014). Light yellow shadings indicate periods of relatively stronger LC while gray shadings indicate periods of relatively weaker LC.

3.2. TEX$_{86}$-based temperatures on the northwest shelf of Australia

Compared to the $U_{37}^{K'}$ proxy, the TEX$_{86}$ index appears to be more complicated, and should be evaluated before applying into a temperature reconstruction (Schouten et al., 2002, 2013). Generally, changes in archaeal ecology and potential terrestrial input usually complicate the relation of temperature and the TEX$_{86}$ index derived from *Thaumarchaeota* (Schouten et al., 2013). However, the MI values at Site U1461 are relatively low (0.19–0.34, Table S1), suggesting minor impact of methanotrophic *Euryarchaeota* to the TEX$_{86}$ index (Zhang et al., 2011). The BIT values vary from 0.07 to 0.46, with 85% of samples lower than 0.3 (Table S1), suggesting that the potential impact from the contribution of terrestrial-derived isoGDGTs would be minor at Site U1461 (Hopmans et al.,

2004; Schouten et al., 2013). After excluding samples with BIT values higher than 0.3, the TEX$_{86}$ index in remaining samples should track temperature changes (Table S1).

At Site U1461, temperatures derived from TEX$_{86}$ vary from 14.6 to 27.8 °C over the last 6 Myr (Fig. 2b, Table S1). Higher TEX$_{86}$-temperatures occurred during the late Miocene and the early Pliocene, whereas lower temperatures during the late Pleistocene (Fig. 2b). Overall, TEX$_{86}$-temperatures at Site U1461 demonstrate a unidirectional decreasing trend over the last 6 Myr (1.0 °C/Myr, $r^2 = 0.56$, $n = 195$). The temperature difference between the U$_{37}^{K'}$-based and TEX$_{86}$-based temperatures, increased over the last 6 Myr (Fig. 2c). The rate of the increasing difference is higher during 1.2–0 Ma (2.2 °C/Myr, $n = 59$) than 6–1.2 Ma (0.5 °C/Myr, $n = 99$).

3.3. Primary productivity on the northwest shelf of Australia

Concentrations of isoGDGTs and C$_{28}$–C$_{30}$ sterols at Site U1461 vary from 0.2 to 358.0 ng/g, and from 12.3 to 2114.9 ng/g over the last 6 Myr, respectively (Fig. 2d, Table S1). Our primary productivity records show an increasing trend during 6–1.2 Ma, coincident with the general cooling trend over the Pliocene-Pleistocene period (Fig. 2). Primary productivity on the northwest shelf of Australia started to decrease after ∼1.2 Ma, opposite to the previous increasing trend during 6–1.2 Ma (Fig. 2d).

4. Discussion

4.1. Proxy interpretations for U$_{37}^{K'}$ and TEX$_{86}$

The U$_{37}^{K'}$ index has been widely applied for pelagic SST reconstructions, with calibration mainly derived from Group III haptophytes, including *Emiliania huxleyi* and *Gephyrocapsa oceanica* (Prahl et al., 1988; Müller et al., 1998). However, its applications might have been hampered by other haptophyte groups (Group I and Group II haptophytes) that potentially related to salinity and nutrient dynamics (Salacup et al., 2019). Most of the C$_{37}$/C$_{38}$ values at Site U1461 range from 0.7 to 1.7, suggesting limited contribution from Group II haptophytes (Fig. S7; Salacup et al., 2019). Also, lack of C$_{37:4}$ alkenone indicates that Group I haptophytes do not contribute measurably to the alkenone inventory at Site U1461 (Fig. S5). Accordingly, alkenones at Site U1461 are primarily produced by Group III haptophytes, different from those at Site U1463 which were largely contaminated by coastal signatures (Group II haptophytes, Salacup et al., 2019; Smith et al., 2020). Although the C$_{37}$/C$_{38}$ values at Site U1461 shift from 0–1 before ∼1.2 Ma to 1–1.5 after ∼1.2 Ma, no obvious correlation can be seen in the C$_{37}$/C$_{38}$ vs. U$_{37}^{K'}$ plot (Fig. S7), suggesting the C$_{37}$/C$_{38}$ values only have negligible impacts on U$_{37}^{K'}$ values.

In recent years, the TEX$_{86}$ index has been interpreted as an SST indicator on the west shelf of Australia through the Pliocene-Pleistocene period (Fig. 1), including Sites U1459 (De Vleeschouwer et al., 2019), U1460 (Petrick et al., 2019) and U1463 (Smith et al., 2020). However, it has also been suggested that the TEX$_{86}$ proxy in many regions, especially at low latitudes and near coastal regions, may reflect the temperature of the subsurface waters or the whole water column rather than just the sea surface, as nitrifying *Thaumarchaeota* in deeper waters contributes to the TEX$_{86}$ signal (Smith et al., 2013; Ho and Laepple, 2016; Kim et al., 2016). In the Australian region, an investigation on surface sediments from the southeastern shelf of Australia suggests that the TEX$_{86}$ proxy is closely correlated with annual temperature in the integrated 0–200 m water depth profile (Smith et al., 2013). Meanwhile, a recent study of core-top sediments from the northwestern shelf of Australia suggests that TEX$_{86}$ might reflect summer SSTs, as TEX$_{86}$-based SSTs inferred by the BAYSPAR (Bayesian, Spatially-Varying Regression) calibration are 3 °C higher than modern mean annual

SST (Tierney and Tingley, 2014; Smith et al., 2020). However, this seasonal bias in the TEX$_{86}$ proxy does not explain the divergent behavior between the TEX$_{86}$ and U$_{37}^{K'}$ proxies after ∼1.2 Ma at Site U1461 (Fig. 2). A cold season bias has to be introduced in order to explain the lack of warming trend after ∼1.2 Ma in the TEX$_{86}$ record, which is in contrast with the inferred warm bias at Site U1463 (Smith et al., 2020). Furthermore, it is even more problematic to explain why the seasonality shift should have occurred around 1.2 Ma. Rather, with production depth taken into consideration, the U$_{37}^{K'}$ proxy at Site U1461 should mainly reflect SST (Prahl et al., 1988; Müller et al., 1998), while the TEX$_{86}$ proxy reflects integrated water column temperature (Smith et al., 2013; Ho and Laepple, 2016; Kim et al., 2016), recording both surface and subsurface signals. The depth of water column that the TEX$_{86}$ may indicate is difficult to be determined, as *Thaumarchaeota* might change their habitat depth under different oceanic settings (Kim et al., 2016).

When putting all the available TEX$_{86}$ records on the northwestern shelf of Australia together, the TEX$_{86}$ values at Sites U1461 and U1463 (Christensen et al., 2017; Smith et al., 2020) resemble each other during 6–2.5 Ma, but show consistently higher values than those from Site U1459 (Fig. S8; De Vleeschouwer et al., 2019). Also, although at extremely low resolution and with large chronological error, the TEX$_{86}$ values at Site U1463 also show a warming pattern after ∼1.5 Ma (Christensen et al., 2017), different with those at Sites U1460 (Petrick et al., 2019) and U1461 but similar to the U$_{37}^{K'}$-based SSTs at Site U1461 (Fig. S8). Therefore, we suggest that the TEX$_{86}$ proxy on the northwestern shelf of Australia still contain signal of surface temperature. The cooling signal in subsurface waters, connected to high-latitude water masses that generally cooled through the Pliocene-Pleistocene period (Caballero-Gill et al., 2019; Peterson et al., 2020), could have diluted the warming signal from surface waters. The warming trend identified in the TEX$_{86}$ values at the equatorward Site U1463 after ∼1.5 Ma (Fig. S8) appears to support this interpretation, as the influence of high-latitude water masses is relatively small. In line with this interpretation, the difference between the U$_{37}^{K'}$- and TEX$_{86}$-temperatures could be used as a qualitative measure of vertical thermal difference. Future work using sediment traps, water column filtering, or genetic techniques is crucial for determining the habitat depth and seasonality of *Thaumarchaeota* on the northwest shelf of Australia (Smith et al., 2020). Nevertheless, the warming trend after ∼1.2 Ma in the U$_{37}^{K'}$ record, in contrast with the cooling trend in many SST records elsewhere (Li et al., 2011; Zhang et al., 2014; Caballero-Gill et al., 2019; Peterson et al., 2020), stands out as a unique feature that points to an additional regional influence.

4.2. Variation of the LC strength through the Pliocene-Pleistocene period

4.2.1. Stronger LC since ∼1.2 Ma

Since ∼1.2 Ma, which is known as the Mid-Pleistocene Transition (MPT, Lisiecki and Raymo, 2005), SSTs at Site U1461 show a warming trend reaching values comparable with the Pliocene SSTs (Fig. 2a). This is in stark contrast to the global cooling trend (Lisiecki and Raymo, 2005; Zhang et al., 2014; Herbert et al., 2016). The higher U$_{37}^{K'}$-SST gradient between the northwest shelf of Australia (Site U1461) and the high latitude Southern Hemisphere (Site 1125, Caballero-Gill et al., 2019; Peterson et al., 2020) indicates that the increasing SSTs at Site U1461 could not be contributed to water masses from high latitude region (Fig. 3b). On the contrary, the SST gradient between the Indo-Pacific Warm Pool (Sites 806 and 1143) and the northwest shelf of Australia (Site U1461) decreased to ∼0 °C after ∼1.2 Ma, suggesting strong connection and communication of surface waters between the two regions (Figs. 3a, S6; Li et al., 2011; Zhang et al., 2014). Therefore, the warmer SSTs on the northwest shelf of Australia after the MPT ap-

pear to suggest a stronger LC. Despite the stronger LC after 1.2 Ma, there is still evidence for slightly cooler conditions at ∼0.65 Ma, probably due to sharp drop of sea levels cutting off some ITF channels (Petrick et al., 2019).

TEX_{86}-based temperatures at Site U1461 show generally lower values after the MPT, different from the $U_{37}^{K'}$-SST pattern (Fig. 2). The vertical thermal difference between the $U_{37}^{K'}$- and TEX_{86}-based temperatures at Site U1461, shows higher values after ∼1.2 Ma than before (Fig. 2c). The enlarged vertical thermal difference might be attributed to the stronger LC by transporting warm surface water from the tropical region and potential increased upwelling by transporting cold water from the subsurface (Feng et al., 2003, 2015). It is also possible that the *Thaumarchaeota* move to deeper layer with cooler temperature due to depressed nutrient on the surface, therefore bringing more subsurface temperature signatures to the TEX_{86} proxy. Nevertheless, the paired $U_{37}^{K'}$ and TEX_{86} records together suggest an increase in the LC strength after ∼1.2 Ma.

At Site U1460, there is also no general increasing feature of TEX_{86}-based temperatures through ∼1.2–0 Ma but rather a substantial increase in glacial-interglacial temperature variability, which was previously attributed to the effect of sea level changes on the ITF dynamics (Fig. S8; Petrick et al., 2019). Interestingly, TEX_{86}-based temperature gradient between Site U1461 and Site U1460 lowered at ∼1.2 Ma by ∼2–3 °C to values of <0 °C (Fig. 3c), further suggesting the complexity of TEX_{86} in temperature reconstruction. The *Thaumarchaeota* at Site U1460 might still live in the upper layer of water column compared to Site U1461, resulting in higher sedimentary TEX_{86} values in higher latitude region (Site U1460). Different habitat depths for the *Thaumarchaeota* between two regions can also be explained by different response of the *Thaumarchaeota* to the strong LC after ∼1.2 Ma. As Site U1460 is located further south than Site U1461, it was less impacted by the warm and nutrient-deficient water from the low latitude areas brought by the strong LC after ∼1.2 Ma. Under this circumstance, the *Thaumarchaeota* might still live in the upper layer of water column at Site U1460, and mainly respond to the global cooling condition. During some glacial phases during ∼1.2–0 Ma (e.g. ∼0.65 Ma; Petrick et al., 2019), the TEX_{86}-based temperature gradient between Site U1461 and Site U1460 increased (Fig. 3c). Other than changes in the habitat depth for the *Thaumarchaeota*, it is also possible that stronger Leeuwin Undercurrent (>200 m deep) in glacial periods decreased the temperatures at Site U1460 to some extent (Petrick et al., 2019), but had nearly no impact on temperatures at Site U1461, further increasing the TEX_{86}-based temperature gradient between Site U1461 and Site U1460.

Furthermore, primary productivity of archaea and algae decreased substantially after ∼1.2 Ma (Fig. 2d). If the LC was in a weak form, pronounced Pliocene-Pleistocene cooling would have intensified upwelling strength on the northwest shelf of Australia, and have increased nutrient availability and primary productivity (Etourneau et al., 2009). Therefore, the suppressed primary productivity in the whole water column after ∼1.2 Ma may indicate stronger LC, which transported additional warm, low-salinity, nutrient-deficient tropical surface water along the west coast of Australia (Pattiaratchi, 2006; Feng et al., 2015). In summary, the surface warming, potential decreased subsurface temperature, and suppressed primary productivity on the northwest shelf of Australia all together suggest a stronger LC since the MPT.

4.2.2. Generally weak LC during 4–1.2 Ma

Compared to ∼1.2–0 Ma, the SST gradient between the Indo-Pacific Warm Pool (Sites 806 and 1143, Li et al., 2011; Zhang et al., 2014) and the northwest shelf of Australia (Site U1461) is ∼1–3 °C higher during 4–1.2 Ma (Fig. 3a). Meanwhile, the SST gradient between the northwest shelf of Australia (Site U1461) and the high

latitude region (Site 1125, Caballero-Gill et al., 2019; Peterson et al., 2020) during 4–1.2 Ma is ∼3–5 °C lower than that after ∼1.2 Ma (Fig. 3b). Both lines of evidence indicate less warm water contribution of the LC from tropical regions to Site U1461. The weak LC condition is also supported by higher primary productivity, probably due to less input of low-salinity, nutrient-deficient tropical surface water (Fig. 3d). Higher differences in TEX_{86}-based temperature between Site U1461 and Site U1460 (Petrick et al., 2019), and between Site U1461 and Site U1459 (De Vleeschouwer et al., 2019) during 4–1.2 Ma might also suggest a relatively weak LC strength, based on our interpretation discussed above (Fig. 3c).

Under the background of the generally weak LC during 4–1.2 Ma, we also observed some periods of much weaker LC conditions, which have been identified previously (Christensen et al., 2017; De Vleeschouwer et al., 2018, 2019; Auer et al., 2019, 2020; Petrick et al., 2019). For instance, the weak LC at ∼1.55 Ma (Fig. 3) is also observed by records from Site U1460 (Petrick et al., 2019) and Site U1463 (Smith et al., 2020). Another weaker LC event at ∼2.5 Ma (Fig. 3) might correspond to the MIS 100 glacial period (Auer et al., 2020). During 3.8–3.3 Ma, records from Site U1461 also show a decrease in the LC strength, consistent with the well-recognized ITF constriction event (Christensen et al., 2017; De Vleeschouwer et al., 2018, 2019; Auer et al., 2019, 2020). However, the variation of the LC strength within 4–1.2 Ma is not as strong as that during ∼1.2–0 Ma (Fig. 3), highlighting the importance of more investigations on the ITF and LC variations in the Pleistocene epoch.

4.2.3. Plausible existence of the LC during 6–4 Ma

The status of the LC during 6–4 Ma is more difficult, due to the lack of other SST records around the region. Although the vertical thermal difference between $U_{37}^{K'}$ and TEX_{86} at Site U1461 was low during 6–4 Ma (Fig. 2c), it might not be sensitive enough to infer the LC strength. It is possible that the TEX_{86} values contain more surface signal and resemble the SST during 6–4 Ma, leading to a small difference between $U_{37}^{K'}$ and TEX_{86}. However, some lines of evidence may still suggest a plausible existence of the LC during 6–4 Ma. Firstly, the Australian continent was further south during 6–4 Ma, allowing the transportation of tropical warm water to the northwest shelf of Australia (Cane and Molnar, 2001; Christensen et al., 2017). On the other hand, the primary productivity at Site U1461 was even lower during 6–4 Ma than that after ∼1.2 Ma (Fig. 2d), perhaps suggesting a relatively low-salinity, nutrient-deficient condition due to the existence of the LC. However, considering the comparable SST conditions during 1.2–0 Ma (globally cooling phase) and 6–4 Ma (globally warming phase), the LC during 6–4 Ma should be weaker than that during 1.2–0 Ma. It is quite possible that the wide opening of Maritime Continent for the stronger ITF during 6–4 Ma didn't induce stronger LC. More SST records around the northwest shelf of Australia are required to further address this issue.

4.3. Triggers for the stronger LC at ∼1.2 Ma

At present, warm surface water sourced from the ITF and along-shore pressure gradient off western Australia are two main contributors to the LC strength (Molnar and Cronin, 2015). Records from Site U1461 seem to support the idea that the ITF strength may not be the main reason for the variation of the LC strength through the Pliocene-Pleistocene period. For instance, our records show a generally weak LC during 4–2 Ma, when the ITF was changing from very strong to restricted conditions due to the decrease of sea level and tectonic geometric reorganization of the Indonesian Gateway system (Christensen et al., 2017; De Vleeschouwer et al., 2018, 2019; Auer et al., 2019, 2020; Smith et al., 2020). Also, at ∼0.65 Ma when decreased sea level significantly restricted the flow pathways of the ITF (Petrick et al., 2019), the LC strength is

comparable to the one at ∼4 Ma, when the sea level was relatively high (Lisiecki and Raymo, 2005) and the ITF was unrestricted and strong (Fig. 3; Christensen et al., 2017). Therefore, the impact of sea level and the ITF strength on the LC strength may exist, but did not dominate the LC variation through the Pliocene-Pleistocene period. Indeed, model simulations suggested that the impacts of the stronger ITF on the SST along the northwest shelf of Australia in the early Pliocene are barely above statistical significance (Fedorov et al., 2013). The main reason for this might be that although some passages (Makassar, Lombok, and Karimata passages) became much shallower since the MPT, there were some main passages deeper than 1000 m (Ombai and Timor passages), continuously providing source water for the LC (Cane and Molnar, 2001; Molnar and Cronin, 2015).

Alternatively, stronger atmospheric circulations might be very important for the stronger LC condition since the MPT. As illustrated by a suite of SST records between the warm western equatorial Pacific and the cold eastern equatorial Pacific, the Walker Circulation strengthened along with the Pliocene-Pleistocene cooling (Fig. 3e; Fedorov et al., 2013; Zhang et al., 2014). Under the prolonged La Niña-like condition, excessive precipitation on the Maritime Continent freshened the surface water in both the western Pacific Ocean and the Indonesian Ocean (Fedorov et al., 2013), enlarging the meridional salinity gradient on the northwest shelf of Australia (Feng et al., 2003). Also, higher meridional SST gradient of the Pacific Ocean (Fig. 3f) may have induced stronger global trade winds and further increased the LC as the compensation of increased west Australian current (Spooner et al., 2011; Fedorov et al., 2013). Therefore, enhanced zonal Walker Circulation and meridional Hadley Circulation may have triggered the stronger LC even under the situation of the relatively restricted ITF (compared to the Pliocene) at ∼1.2 Ma.

4.4. Impacts of the stronger LC on climates in northwestern Australia after ∼1.2 Ma

There exists a major transition from a cool and dry climate in the late Miocene to a warm and humid phase in the early Pliocene on the northwestern Australian continent (Sniderman et al., 2016; Christensen et al., 2017; Groeneveld et al., 2017; Fig. 4d). This humid phase occurred when the Western Pacific Warm Pool expanded west to the South China Sea (Zhang et al., 2014) and the eastern Indian Ocean (Karas et al., 2011). Warmer waters surrounding the northwestern Australian continent may have provided more moisture supply for the development and persistence of the humid phase over the early Pliocene (Sniderman et al., 2016; Christensen et al., 2017). Moisture availability in the northwestern Australia reduced during 4–3 Ma, consistent with lower terrigenous input to the northwestern Australian shelf (Sites ODP 762 and U1463; Figs. 4c, 4d; Christensen et al., 2017; Stuut et al., 2019). The general aridification in north and west Australia is synchronous with the expansion of C4 plants over C3 plants, which is attributed to increased seasonality of precipitation from the onset of the Australian monsoon regime (Andrae et al., 2018). Therefore, the aridification in northwestern Australia through the Pliocene may be induced by less moisture supply due to restricted ITF under the ongoing tectonic reorganization on the Maritime Continent (Krebs et al., 2011; Sniderman et al., 2016; Christensen et al., 2017; Stuut et al., 2019), as well as changes in the global atmospheric circulations (Brierley et al., 2009; Fedorov et al., 2013; Andrae et al., 2018).

After ∼1.2 Ma, the stronger LC induced a warm SST condition at Site U1461 comparable to the early Pliocene (Fig. 2a), but didn't lead to generally wet conditions observed in the early Pliocene (Figs. 4c, 4d; Krebs et al., 2011; Sniderman et al., 2016; Christensen et al., 2017; Stuut et al., 2019). On the contrary, many studies have
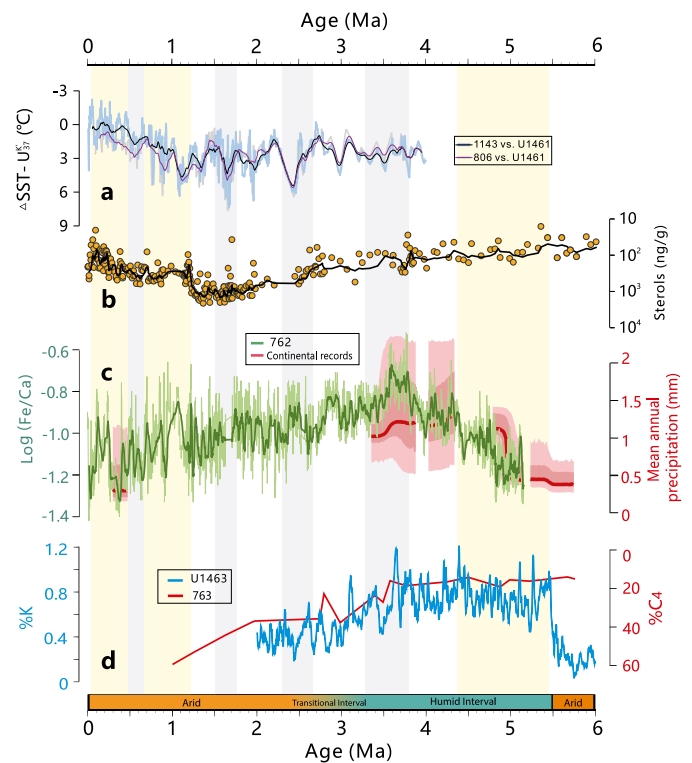
Fig. 4. Comparison of the LC development with climates on the northwest shelf of Australia over the last 6 Myr. (a) Differences of $U_{37}^{K'}$-based SST between Site 1143 (Li et al., 2011) and Site U1461 (blue lines with black 0.1 Ma smoothing curves), and between Site 806 (Zhang et al., 2014) and Site U1461 (gray lines with purple 0.1 Ma smoothing curves) over the last 4 Myr. (b) Concentrations of C_{28}-C_{30} sterols from Site U1461 with 3-point smoothing curves over the last 6 Myr (in reversed scale). (c) Mean annual precipitation variation in southern Australia based on Monte Carlo simulations on the continental vegetation change (red lines, Sniderman et al., 2016), and precipitation variation in northwestern Australia based on Log (Fe/Ca) record from Site 762 (green lines, Stuut et al., 2019; with updated chronology by Auer et al., 2020). (d) River runoff and terrigenous input in northwestern Australia based on percentage of potassium (%K) from site U1463 (blue lines, Christensen et al., 2017; with updated chronology by Auer et al., 2020), and C4 plant coverage (%C4) in northwestern Australia based on $\delta^{13}C$ values of n-C_{31} alkane from Site 763 (red lines, Andrae et al., 2018). Light yellow shadings indicate periods of relatively stronger LC while gray shadings indicate periods of relatively weaker LC. A summary of climate variation in northwestern Australia was shown at the bottom (Christensen et al., 2017; Auer et al., 2019, 2020; De Vleeschouwer et al., 2019).

proposed a generally drier condition in northwestern and southeastern Australia since 1.5–1.0 Ma (McLaren and Wallace, 2010; Sniderman, 2011; Sniderman et al., 2016; Stuut et al., 2019). Model simulations suggested that changes in the Hadley circulation and the Walker circulation may have caused drier environmental conditions in regions adjacent to eastern boundary currents (Brierley et al., 2009). As the meridional temperature contrast increased and the Hadley cell intensified after the MPT, a stronger atmospheric subsidence would lead to the aridification of the western Australian continent (Fedorov et al., 2013). Therefore, climates on the western Australian continent were mainly modulated by the atmospheric circulations associated with the global Pliocene-Pleistocene cooling, while the influence of the stronger LC and the corresponding warm SST on this long-term drying trend was perhaps secondary.

Since the MPT, large glacial-interglacial oscillations become an important signature in the climatic setting of the northwestern Australian area (Gallagher et al., 2009; Spooner et al., 2011). Although the northwestern Australian continent was generally dry, moisture availabilities during some interglacial periods over the late Pleistocene could be comparable with those in the early Pliocene (Site 762; Fig. 4c; Stuut et al., 2019). It is possible

that during the interglacial periods over the late Pleistocene, the stronger LC potentially contributed to the wetness over the northwestern Australian continent by providing more moisture availability and enhancing austral summer monsoon (Molnar and Cronin, 2015). This is perhaps the reason for large-amplitude hydrological swings on the Australian continent on orbital scales over the late Pleistocene (Gallagher et al., 2009; Spooner et al., 2011). Therefore, although the intensified LC after ∼1.2 Ma may have potentially brought additional moisture to the northwestern Australian continent during the interglacial periods over the late Pleistocene, it could not overturn the long-term drying trend associated with the global cooling over the Pliocene-Pleistocene period.

5. Conclusions

The $U^{K'}_{37}$-SST record at Site U1461 on the northwest shelf of Australia suggests a progressive warming trend after ∼1.2 Ma, in contrast with the long-term global cooling trend. The $U^{K'}_{37}$-SST values are comparable to those in the Indo-Pacific Warm Pool, suggesting strong connection and communication of surface waters between the two regions. The regional surface warming and suppressed primary productivity on the northwest shelf of Australia together indicate prevailing warm, low-salinity, nutrient-deficient surface water, and thus a stronger LC since the MPT. During 4–1.2 Ma, higher temperature gradient between the Indo-Pacific Warm Pool and the northwest shelf of Australia, and increased primary productivity indicate a generally weaker LC condition. Warmer temperatures and lower productivity suggest a plausible existence of a weak LC during 6–4 Ma, but more work is required to confirm this. The variation of the LC strength through the Pliocene-Pleistocene period differs from the sea level and the ITF variations, suggesting that the sea level and the ITF strength may not be the main reason for the LC variation. Alternatively, the stronger LC after ∼1.2 Ma was more likely triggered by enhanced atmospheric circulation. Although the intensified LC may have potentially brought additional moisture to the Australian continent during the interglacial periods over the late Pleistocene, it has not overturned the long-term drying trend over the Pliocene-Pleistocene period.

CRediT authorship contribution statement

Yuxin He: Conceptualization, Funding acquisition, Investigation, Methodology, Writing – original draft, Writing – review & editing. **Huanye Wang:** Methodology, Writing – original draft, Writing – review & editing. **Zhonghui Liu:** Writing – original draft, Writing – review & editing.

Declaration of competing interest

The authors declare that they have no known competing financial interests or personal relationships that could have appeared to influence the work reported in this paper.

Acknowledgements

Appendix A. Supplementary material

Supplementary material related to this article can be found online at https://doi.org/10.1016/j.epsl.2021.116767.

References

Andrae, J.W., et al., 2018. Initial expansion of C4 vegetation in Australia during the late Pliocene. Geophys. Res. Lett. 45, 4831–4840.

Auer, G., De Vleeschouwer, D., Christensen, B.A., 2020. Towards a robust Plio-Pleistocene chronostratigraphy for ODP Site 762. Geophys. Res. Lett. 47, e2019GL085198.

Auer, G., et al., 2019. Timing and pacing of Indonesian Throughflow restriction and its connection to late Pliocene climate shifts. Paleoceanogr. Paleoclimatol. 34, 635–657.

Brierley, C.M., Fedorov, A.V., Liu, Z., Herbert, T.D., Lawrence, K.T., LaRiviere, J.P., 2009. Greatly expanded tropical warm pool and weakened Hadley circulation in the early Pliocene. Science 323, 1714–1718.

Caballero-Gill, R.P., Herbert, T.D., Dowsett, H.J., 2019. 100-kyr paced climate change in the Pliocene warm period, Southwest Pacific. Paleoceanogr. Paleoclimatol. 34, 524–545.

Cane, M.A., Molnar, P., 2001. Closing of the Indonesian seaway as a precursor to East African aridification around 3–4 million years ago. Nature 411, 157–162.

Christensen, B.A., et al., 2017. Indonesian Throughflow drove Australian climate from humid Pliocene to arid Pleistocene. Geophys. Res. Lett. 44, 6914–6925.

De Vleeschouwer, et al., 2018. The amplifying effect of Indonesian Throughflow heat transport on late Pliocene Southern Hemisphere climate cooling. Earth Planet. Sci. Lett. 500, 15–27.

De Vleeschouwer, D., Petrick, B.F., Martínez-García, A., 2019. Stepwise weakening of the Pliocene Leeuwin Current. Geophys. Res. Lett. 46, 8310–8319.

Etourneau, J., Martinez, P., Blanz, T., Schneider, R., 2009. Pliocene-Pleistocene variability of upwelling activity, productivity, and nutrient cycling in the Benguela region. Geology 37, 871–874.

Fedorov, A.V., Brierley, C.M., Lawrence, K.T., Liu, Z., Dekens, P.S., Ravelo, A.C., 2013. Patterns and mechanisms of early Pliocene warmth. Nature 496, 43–49.

Feng, M., Benthuysen, J., Zhang, N., Slawinski, D., 2015. Freshening anomalies in the Indonesian Throughflow and impacts on the Leeuwin Current during 2010-2011. Geophys. Res. Lett. 42, 8555–8562.

Feng, M., Meyers, G., Pearce, A., Wijffels, S., 2003. Annual and interannual variations of the Leeuwin Current at 32°S. J. Geophys. Res. 108, 3355.

Gallagher, S.J., et al., 2009. Neogene history of the West Pacific Warm Pool, Kuroshio and Leeuwin currents. Paleoceanography 24, PA1206.

Gallagher, S.J., et al., 2018. The enigma of rare Quaternary oolites in the Indian and Pacific Oceans: a result of global oceanographic physicochemical conditions or a sampling bias? Quat. Sci. Rev. 200, 114–122.

Gallagher, S.J., Fulthorpe, C.S., Bogus, K., the Expedition 356 Scientists, 2017. Indonesian Throughflow. International Ocean Discovery Program, College Station, TX.

Gordon, A.L., 2005. Oceanography of the Indonesian seas and their throughflow. Oceanography 18, 14–27.

Groeneveld, J., et al., 2017. Australian shelf sediments reveal shifts in Miocene Southern Hemisphere Westerlies. Sci. Adv. 3, e1602567.

Hallenberger, M., Reuning, L., Gallagher, S.J., Back, S., Ishiwa, T., Christensen, B.A., Bogus, K., 2019. Increased fluvial runoff terminated inorganic aragonite precipitation on the Northwest Shelf of Australia during the early Holocene. Sci. Rep. 9, 18356.

Herbert, T.D., Lawrence, K.T., Tzanova, A., Peterson, L.C., Caballero-Gill, R., Kelly, C.S., 2016. Late Miocene global cooling and the rise of modern ecosystems. Nat. Geosci. 9, 843–847.

Ho, S.L., Laepple, T., 2016. Flat meridional temperature gradient in the early Eocene in the subsurface rather than surface ocean. Nat. Geosci. 9, 606–610.

Hopmans, E.C., et al., 2004. A novel proxy for terrestrial organic matter in sediments based on branched and isoprenoid tetraether lipids. Earth Planet. Sci. Lett. 224, 107–116.

Ishiwa, T., Yokoyama, Y., Reuning, L., McHugh, C.M., De Vleeschouwer, D., Gallagher, S.J., 2019. Australian summer monsoon variability in the past 14,000 years revealed by IODP expedition 356 sediments. Prog. Earth Planet. Sci. 6, 17.

Karas, C., Nürnberg, D., Tiedemann, R., Garbe-Schönberg, D., 2011. Pliocene Indonesian Throughflow and Leeuwin Current dynamics: implications for Indian Ocean polar heat flux. Paleoceanography 26, PA2217.

Kim, J.H., Villanueva, L., Zell, C., Sinninghe Damsté, J.S., 2016. Biological source and provenance of deep-water derived isoprenoid tetraether lipids along the Portuguese continental margin. Geochim. Cosmochim. Acta 172, 177–204.

Krebs, U., Park, W., Schneider, B., 2011. Pliocene aridification of Australia caused by tectonically induced weakening of the Indonesian Throughflow. Palaeogeogr. Palaeoclimatol. Palaeoecol. 309, 111–117.

Lawrence, K.T., Woodard, S.C., 2017. Past sea surface temperatures as measured by different proxies-a cautionary tale from the late Pliocene. Paleoceanography 32, 318–324.

Li, L., Li, Q., Tian, J., Wang, P., Wang, H., Liu, Z., 2011. A 4-Ma record of thermal evolution in the tropical western Pacific and its implications on climate change. Earth Planet. Sci. Lett. 309, 10–20.

Lisiecki, L.E., Raymo, M.E., 2005. A Pliocene-Pleistocene stack of 57 globally distributed benthic δ^{18}O records. Paleoceanography 20, PA1003.

McLaren, S., Wallace, M.W., 2010. Plio-Pleistocene climate change and the onset of aridity in southeastern Australia. Glob. Planet. Change 71, 55–72.

Molnar, P., Cronin, T.W., 2015. Growth of the Maritime Continent and its possible contribution to recurring ice ages. Paleoceanography 30, 196–225.

Morrow, R., Fang, F., Fieux, M., Molcard, R., 2003. Anatomy of three warm-core Leeuwin Current eddies. Deep-Sea Res., Part II 50, 2229–2243.

Müller, P.J., Kirst, G., Ruhland, G., Storch, I., Rosell-Mele, A., 1998. Calibration of the alkenone paleotemperature index $U_{37}^{K'}$, based on core-tops from the eastern South Atlantic and the global ocean (60°N–60°S). Geochim. Cosmochim. Acta 62, 1757–1772.

Pattiaratchi, C., 2006. Surface and sub-surface circulation and water masses off Western Australia. Bull. Aust. Meteorol. Oceanogr. Soc. 19, 95–104.

Peterson, L.C., et al., 2020. Plio-Pleistocene hemispheric (a)symmetries in the Northern and Southern Hemisphere midlatitudes. Paleoceanogr. Paleoclimatol. 35, e2019PA003720.

Petrick, B., et al., 2019. Glacial Indonesian Throughflow weakening across the Mid-Pleistocene Climatic Transition. Sci. Rep. 9, 16995.

Prahl, F.G., Muehlhausen, L.A., Zahnle, D.L., 1988. Further evaluation of long-chain alkenones as indicators of paleoceanographic conditions. Geochim. Cosmochim. Acta 52, 2303–2310.

Salacup, J.M., Farmer, J.R., Herbert, T.D., Prell, W.L., 2019. Alkenone paleothermometry in coastal settings: evaluating the potential for highly resolved time series of sea surface temperature. Paleoceanogr. Paleoclimatol. 34, 164–181.

Schouten, S., et al., 2002. Distributional variations in marine crenarchaeotal membrane lipids: a new tool for reconstructing ancient sea water temperatures? Earth Planet. Sci. Lett. 204, 265–274.

Schouten, S., Hopmans, E.C., Sinninghe Damsté, J.S., 2013. The organic geochemistry of glycerol dialkyl glycerol tetraether lipids: a review. Org. Geochem. 54, 19–61.

Smith, M., et al., 2013. Comparison of $U_{37}^{K'}$, TEX_{86}^{H} and LDI temperature proxies for reconstruction of South-East Australian ocean temperatures. Org. Geochem. 64, 94–104.

Smith, R.A., et al., 2020. Plio-Pleistocene Indonesian Throughflow variability drove Eastern Indian Ocean sea surface temperatures. Paleoceanogr. Paleoclimatol. 35, e2020PA003872.

Sniderman, J.M.K., 2011. Early Pleistocene vegetation change in upland south-eastern Australia. J. Biogeogr. 38, 1456–1470.

Sniderman, J.M.K., et al., 2016. Pliocene reversal of late Neogene aridification. Proc. Natl. Acad. Sci. USA 113, 1999–2004.

Stuut, J.B.W., et al., 2019. A 5.3-million-year history of monsoonal precipitation in northwestern Australia. Geophys. Res. Lett. 46, 6946–6954.

Spooner, M.I., De Deckker, P., Barrows, T.T., Fifield, L.K., 2011. The behaviour of the Leeuwin Current offshore NW Australia during the last five glacial–interglacial cycles. Glob. Planet. Change 75, 119–132.

Tierney, J.E., Tingley, M.P., 2014. A Bayesian, spatially-varying calibration model for the TEX_{86} proxy. Geochim. Cosmochim. Acta 127, 83–106.

Volkman, J.K., Barrett, S.M., Blackburn, S.I., Mansour, M.P., Gelin, F., 1998. Microalgal biomarkers: a review of recent research developments. Org. Geochem. 29, 1163–1179.

Zhang, Y., Pagani, M., Liu, Z., 2014. A 12-million-year temperature history of the tropical Pacific Ocean. Science 344, 84–87.

Zhang, Y., Zhang, C., Liu, X., Li, L., Hinrichs, K.U., Noakes, J.E., 2011. Methane index: a tetraether archaeal lipid biomarker indicator for detecting the instability of marine gas hydrates. Earth Planet. Sci. Lett. 307, 525–534.